MondoScience
Est 2016

Modern Materials: Two-Dimensional Materials

Continuing Education for Professional Engineers

PREPARED BY :
MondoScience

CONTACT :
Online-PDH, Cadistics, LLC
www.online-pdh.com
Email: cadistics@yahoo.com

Course Description

This course provides engineers with a comprehensive introduction to two-dimensional (2D) materials, a class of modern materials that includes graphene, hexagonal boron nitride (h-BN), transition metal dichalcogenides (TMDs), MXenes, and phosphorene. The course explores their synthesis routes, fundamental structure–property relationships, device integration pathways, and large-scale applications across electrical, optical, chemical, and structural domains.

Participants will gain a strong foundation in the governing models and equations used to describe mechanical reinforcement, thermal transport, electronic behavior, catalytic activity, and membrane performance. Case studies and worked examples are incorporated to connect theory with practical engineering applications in electronics, energy systems, composites, coatings, and membranes. The course also addresses crucial aspects of reliability, environmental health and safety (EHS), and lifecycle considerations, ensuring that learners understand both the opportunities and the challenges of deploying 2D materials in real-world systems.

The course equips professionals to critically assess vendor claims, design materials-based solutions, and anticipate future developments in this rapidly advancing field.

Learning Objectives

By the end of the course, participants will be able to:

- Identify and classify major families of 2D materials, explaining their distinct bonding, structural, and property characteristics.
- Compare and evaluate different synthesis and processing routes (exfoliation, CVD, ALD, solution chemistry) in terms of quality, scalability, and cost.
- Apply governing equations (e.g., Fourier’s law, Halpin–Tsai, Butler–Volmer, percolation theory, skin depth relations) to calculate and predict performance in engineering contexts.
- Interpret characterization data from Raman spectroscopy, TEM, AFM, and electrical/thermal testing to assess material quality.
- Assess device applications of 2D materials in electronics, optoelectronics, EMI shielding, energy storage, catalysis, and membranes.
- Evaluate composites and coatings enhanced with 2D materials, considering reinforcement, conductivity, barrier protection, and tribological performance.
- Analyze reliability, EHS, and lifecycle challenges, including degradation mechanisms, occupational safety, and environmental impacts.

- Understand standardization and market trends influencing adoption of 2D materials in industrial sectors.

Intended Audience

This course is intended for professional engineers working in disciplines such as materials engineering, mechanical engineering, chemical engineering, electrical and electronic engineering, civil and structural engineering, and aerospace engineering. It is suitable for engineers involved in R&D, product design, manufacturing, quality assurance, or regulatory compliance, who require both a strong technical foundation and applied understanding of modern materials.

Table of Contents

Chapter 1: Landscape & Taxonomy of Two-Dimensional Materials

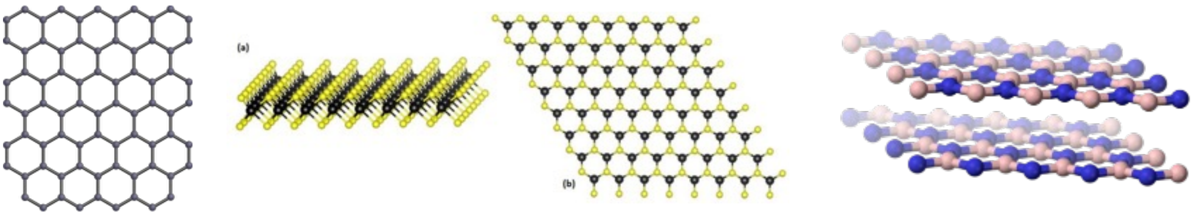

(a) Graphene

(b) Crystal structure of a monolayer of transition metal dichalcogenide

(c) Hexagonal boron-nitride

Figure 1: Two-dimensional (2D) materials

Credit: (b) 3113Ian at English Wikipedia, via Wikimedia Commons

Two-dimensional (2D) materials are crystalline solids with atomic-scale thickness (one to a few layers) and macroscopic lateral dimensions. Their reduced dimensionality yields extreme surface-to-volume ratio, modified phonon and electron dispersions, and property anisotropies that can be exploited in sensing, thermal management, barrier coatings, membranes, energy devices, and electronics.

The field accelerated after the experimental isolation and electrical gating of monolayer graphene, which revealed room-temperature, gate-tunable conduction and ballistic transport over sub-micron distances (Novoselov *et al.*, 2004). Foundational reviews and perspective articles consolidated the materials landscape and highlighted application vectors in the ensuing years (Geim and Novoselov, 2007; Geim and Grigorieva, 2013).

For professional engineers, the practical question is not only **what** 2D materials exist, but **which families map to which performance envelopes**, at what cost and scale, under what standards terminology, and with what stability constraints. This chapter builds a taxonomy that engineers can use to navigate supplier datasheets, select materials for design studies, and plan characterization for acceptance.

Definitions and Scope

A **2D material** is a crystalline solid with strong in-plane bonding and weak interlayer interactions such that a single layer is stable and exhibits distinct properties from the bulk. ISO/TS 80004-13 provides harmonized vocabulary for graphene and related 2D materials, including production terminology (ISO, 2024).

In engineering practice, distinguish is made between:

- **Exfoliable layered crystals** (e.g., graphite → graphene; MoS_2; h-BN; MAX phases → MXenes).
- **Non-layered monolayers grown epitaxially** (e.g., some 2D oxides), which are in scope when they present monolayer-like physics and processing behaviors.

A working geometric descriptor useful for scale analysis is the surface-to-volume ratio for a thin sheet of thickness t and large lateral dimension L (with $L \gg t$): $S/V \approx 2/t$.

Key: S = surface area [m^2], V = volume [m^3], t = thickness [m].

This relation emphasizes that even a few-nanometer increase in thickness can substantially change interfacial reactivity, adsorption, and barrier performance.

Historical Notes and Keystone Results

Graphene, monolayer sp^2 carbon on a honeycomb lattice, was isolated and electrostatically gated to reveal ambipolar transport and high room-temperature mobility (Novoselov *et al.*, 2004; Figure 1(a)). Subsequent reviews established a canonical property set and potential applications ranging from transparent conductors to composites (Geim and Novoselov, 2007). Raman spectroscopy rapidly became the principal, non-destructive probe for layer number, disorder, doping, and strain in sp^2 carbons (Ferrari and Basko, 2013).

Transition-metal dichalcogenides (TMDs), such as molybdenum disulfide (MoS_2; Figure 1 (b)), showed a thickness-driven transition from an indirect bandgap in the bulk to a direct bandgap in monolayer form near ~1.8 eV, enabling efficient photoluminescence and optoelectronic devices (Mak *et al.*, 2010).

Hexagonal boron nitride (h-BN) provided an atomically flat, wide-bandgap (~6 eV) dielectric and UV-emitting material with exceptional chemical stability (Watanabe *et al.*, 2004; Figure 1 (c)).

Phosphorene (few-layer black phosphorus) introduced a p-type 2D semiconductor with anisotropic transport and a layer-dependent direct bandgap (~0.3–2 eV), demonstrated in FETs and simple CMOS inverters (Li *et al.*, 2014; Liu *et al.*, 2014).

MXenes, 2D transition-metal carbides/nitrides, emerged via selective etching of MAX phases (e.g., $Ti_3AlC_2 \rightarrow Ti_3C_2T_x$) and exhibit metallic conductivity, hydrophilicity, and processability as inks and films (Naguib *et al.*, 2011; Anasori *et al.*, 2017). Conductivities exceeding 10,000–19,000 S cm^{-1} have been reported for optimized $Ti_3C_2T_x$ films (Anasori *et al.*, 2017; Guo *et al.*, 2023).

A Taxonomy for Engineering Selection

Families and archetypes

We group 2D materials into families with characteristic bonding, electronic type, and processing routes:

- **Graphitic carbons:** graphene, graphene oxide (GO), reduced GO (rGO). Broadly semi-metallic (graphene), with GO offering tunable oxygen functionality and processability. Benchmark in-plane stiffness (~1 TPa) and high thermal conductivity (> 2,000 W m^{-1} K^{-1}) underpin thermal spreaders and composites (Lee *et al.*, 2008; Balandin, 2011).
- **h-BN:** insulating, polar covalent; excellent dielectric and substrate for low-noise graphene/TMD devices; direct UV gap (~6 eV) (Watanabe *et al.*, 2004).
- **TMDs (e.g., MoS_2, WS_2, WSe_2):** semiconducting monolayers with direct gaps (~1–2 eV) and strong excitonic effects; rich surface chemistry enables catalysis and sensing (Chhowalla *et al.*, 2013; Mak *et al.*, 2010).
- **Group-V 2D (phosphorene, arsenene, antimonene):** p-type behavior common; anisotropic mechanics and transport; bandgap tunable with thickness and strain (Li *et al.*, 2014; Liu *et al.*, 2014).
- **MXenes:** metallic/degenerate semiconducting carbides/nitrides ($M_{n+1}X_nT_x$) with surface terminations (–O/–OH/–F) dictating work function, hydrophilicity, and interfacial chemistry; processable as aqueous inks; suitable for EMI, electrodes, and heaters (Naguib *et al.*, 2011; Anasori *et al.*, 2017).

Electronic type and thickness effects

Electronic structure near the Fermi level determines application fit. Near the K/K′ points, graphene exhibits a linear dispersion:

$$E(\mathbf{k}) = \hbar v_F |\mathbf{k}|$$

(semi-metallic, zero bandgap), supporting high carrier velocities but complicating digital switching;

Key:

E = energy [J]
k = wavevector [m^{-1}]
$\hbar$ = reduced Planck constant [J·s]
v_F = Fermi velocity [m·s^{-1}].

Raman and transport signatures evolve with doping, strain, and disorder (Ferrari and Basko, 2013).

In contrast, monolayer MoS_2 exhibits a **direct bandgap** near ~1.8 eV, transitioning from an **indirect** gap in thicker layers; photoluminescence quantum yield increases by orders of magnitude at monolayer thickness, enabling efficient optoelectronics (Mak *et al.*, 2010). Phosphorene's gap increases as thickness decreases and is highly anisotropic, with mobility and optical absorption depending on crystal orientation (Li *et al.*, 2014; Liu *et al.*, 2014).

Standards and terminology

To avoid ambiguity in specifications and supplier QA, engineers should adopt ISO/TS 80004-13 vocabulary for layer number (monolayer, few-layer, multilayer), flake, film, and related production and property terms, and IEC TS 62607-6 series for graphene-based **key control characteristics** (e.g., sheet resistance by four-point probe or van der Pauw; order parameter by XRD/TEM; functional groups by TGA-FTIR; elemental composition by XPS) (ISO, 2024; IEC, 2022–2024). This terminology underpins procurement, acceptance testing, and cross-supplier comparability.

Property–Application Map

Many 2D materials share **high in-plane stiffness** and **weak out-of-plane coupling**, leading to extreme anisotropy. Graphene combines ~1 TPa Young's modulus and very high in-plane thermal conductivity, which suits thermal spreaders and EMI/ESD layers when paired with suitable conductors or hybrid stacks (Lee *et al.*, 2008; Balandin, 2011). h-BN's chemical and dielectric stability make it valuable as a substrate and encapsulant. TMD monolayers suit low-power electronics and photonics due to their direct gaps and strong excitonic effects (Mak *et al.*, 2010; Chhowalla *et al.*, 2013).

MXenes provide exceptional DC conductivity and processability for printed heaters, antennas, and EMI shielding; optimized transparent films of $Ti_3C_2T_x$ have reported $\sigma > 1.9\times10^4$ S cm^{-1} (Guo *et al.*, 2023). Graphene oxide laminates exhibit unusual water permeation selectivity, relevant to membranes and barrier layers (Nair *et al.*, 2012).

Formula (transport cross-check): for a 2D conductor of *N* squares, total resistance is:

$$R = R_s \times N$$

Where:

R = resistance [Ω]

R_s = sheet resistance [Ω/sq]

N = number of unit squares (geometry).

When paired with mobility $\mu = \sigma/(nq)$, where σ is conductivity [Sm^{-1}], n carrier density [m^{-3}] (or [m^{-2}] in 2D), and q elementary charge [C], engineers can reconcile datasheet claims against measured I–V and Hall data.

Before choosing a material family, it is useful to compare headline properties and archetypal use-cases.

The comparison in Table 1 highlights how electronic type and stability steer applications: h-BN for dielectrics/encapsulation; TMDs/phosphorene for semiconducting/optoelectronic roles; graphene/MXenes for conductive/thermal/EMI functions.

Practical Selection Notes

1. **Specifications must be tied to standards:** request layer number, lateral size distribution, defect/functional group metrics, and electrical/optical properties measured per IEC TS 62607-6 where applicable (IEC, 2022–2024).
2. **CVD vs exfoliation vs chemical routes:** CVD yields wafer-scale films suited to transparent conductors and device stacks; liquid-phase exfoliation supplies inks/flakes for printed conductors/composites (Coleman *et al.*, 2011).
3. **Environmental stability:** phosphorene requires encapsulation; MXenes may oxidize depending on surface terminations and storage; graphene/h-BN are comparatively robust (Anasori *et al.*, 2017).
4. **Measurement cross-checks:** corroborate Raman layer/defect metrics with AFM/XPS and transport via van der Pauw/four-point-probe following IEC guidance (Ferrari and Basko, 2013; IEC, 2022–2024).

Worked Micro-Example: Reconciling Datasheet Claims

A supplier quotes a $Ti_3C_2T_x$ film with transmittance 85 % at 550 nm and sheet resistance 60 Ω/sq. Independent literature reports transparent MXene films with DC conductivity σ up to 1.93×10^4 $S\,cm^{-1}$ (Guo *et al.*, 2023).

Using $R = R_s N$ and $\mu = \sigma/(nq)$ with a plausible 2D carrier density n, an engineer can quickly flag whether the claimed R_s aligns with thickness-dependent σ and transmittance trends reported for optimized films.

Key: R_s [Ω/sq], N [number of unit sqs], μ [$m^2\,V^{-1}\,s^{-1}$], σ [$S\,m^{-1}$], n [m^{-2}], q [C].

Table 1: Property comparison across key 2D families

Family (archetype)	Electronic type	Typical monolayer bandgap	Hallmarks (selected)	Representative applications	Indicative references
Graphene	Semimetal (zero gap)	~0 eV	~1 TPa in-plane modulus; $k > 2{,}000\ W\ m^{-1}\ K^{-1}$; high μ	Transparent conductors, thermal spreaders, composites, RF/ESD	(Geim and Novoselov, 2007; Lee *et al.*, 2008; Balandin, 2011)
h-BN	Insulator	~5.8–6.1 eV	Chemically/thermally robust; atomically flat; good dielectric	Encapsulation, gate dielectrics, UV emitters	(Watanabe *et al.*, 2004)
MoS_2 (TMD)	Semiconductor (direct in ML)	~1.8–1.9 eV	Strong PL in monolayer; excitons; valley physics	FETs, photodetectors/LEDs, sensors	(Mak *et al.*, 2010; Chhowalla *et al.*, 2013)
Phosphorene	Semiconductor (direct)	~0.3–2 eV (thickness-dependent)	Anisotropic transport/optics; p-type	FETs, IR photonics, sensors	(Li *et al.*, 2014; Liu *et al.*, 2014)
$Ti_3C_2T_x$ (MXene)	Metallic/degenerate	~0 eV (metal-like)	Hydrophilic; σ up to ~$1–2\times10^4\ S\ cm^{-1}$ in optimized films	EMI shields, heaters, antennas, electrodes	(Anasori *et al.*, 2017; Guo *et al.*, 2023)

Conclusion

The 2D materials landscape spans insulating h-BN, semiconducting TMDs and phosphorene, and metallic graphene/MXenes, each with distinct processing windows and reliability considerations. ISO/IEC terminology provides a common language to specify layer number, functional groups, and electrical metrics, enabling meaningful vendor comparisons and QC gating. For design, the decisive filters are electronic type, stability, and manufacturability: graphene/h-BN set the foundation for conductive/thermal and dielectric roles; TMDs and phosphorene enable semiconducting/optoelectronic functions; and MXenes extend printable, high-conductivity options for EMI, antennas, and heaters. With the taxonomy and property map established here, subsequent chapters will focus on synthesis, metrology, scale-up, and device-level design rules.

Chapter 2: Synthesis & Processing Routes of Two-Dimensional Materials

Figure 2: Early TEM image of LPE graphene

Credit: Nesbit1973, via Wikimedia Commons

The promise of two-dimensional (2D) materials for electronics, energy, membranes, and composites depends not only on their intrinsic physics but also on the feasibility of producing them at relevant scale, cost, and quality. Engineering practice requires moving beyond laboratory-scale micromechanical exfoliation to reproducible, scalable processes compatible with industrial integration.

The routes to 2D materials fall broadly into top-down exfoliation methods and bottom-up synthetic growth techniques, each with distinct advantages, limitations, and quality footprints. This chapter provides an in-depth review of the dominant synthesis and processing approaches, their mechanisms, control parameters, and implications for device integration.

Top-Down Exfoliation Methods

Mechanical exfoliation

Mechanical exfoliation, famously Scotch tape cleavage of graphite, remains the benchmark for obtaining pristine monolayers with minimal defects and large lateral dimensions (>10 μm). It enabled the first demonstrations of graphene's electronic properties (Novoselov *et al.*, 2004). However, yields are low and flake size is poorly controlled, limiting scalability. For engineers, mechanically exfoliated samples are best reserved for prototyping and fundamental studies where material quality supersedes throughput.

Liquid-phase exfoliation (LPE)

LPE disperses layered crystals in solvents under ultrasonication, shear mixing, or microfluidization, producing dispersions of nanosheets. Solvent choice is critical; surface energy matching between solvent and 2D material minimizes exfoliation energy (Coleman *et al.*, 2011). Stabilizers such as surfactants or polymers prevent reaggregation.

Centrifugation fractionates dispersions by flake size and thickness. Typical yields reach gram-scale per liter, suitable for inks, coatings, and composites, albeit with defect introduction and lateral dimensions usually <1 μm. Optimization involves balancing exfoliation energy, solvent toxicity, and post-processing costs.

Equation (surface energy criterion):

Exfoliation efficiency scales when solvent surface tension

$$\gamma_s \approx \text{nanosheet surface energy } \gamma_f.$$

Key:

γ_s = solvent surface tension [mJ m^{-2}]

γ_f = flake surface energy [mJ m^{-2}].

Electrochemical and intercalation methods

Electrochemical intercalation inserts ions or molecules between layers, expanding interlayer spacing and facilitating exfoliation. For example, lithium intercalation in graphite yields graphene sheets after subsequent exfoliation (Zhao *et al.*, 2011). These methods offer higher yield but introduce chemical residues, requiring thorough washing and annealing.

Bottom-Up Growth Methods

Chemical vapor deposition (CVD)

CVD produces wafer-scale monolayers of graphene, h-BN, and TMDs. Hydrocarbon precursors (e.g., methane) decompose on Cu or Ni substrates to form graphene monolayers with domain sizes dependent on temperature, flow, and pressure (Li *et al.*, 2009). For TMDs, volatile metal oxides and chalcogen vapors co-sublime and nucleate on substrates, with domain orientation influenced by lattice mismatch. Advantages include large area and compatibility with device processing. Challenges include domain boundaries, wrinkles, and the need for transfer to insulating substrates.

Equation (growth rate):

$$r = k \cdot \exp(-E_a/RT)$$

where:

r = deposition rate [nm s^{-1}]
k = pre-exponential factor
E_a = activation energy [J mol^{-1}]
R = gas constant
T = temperature [K].

This Arrhenius dependence governs nucleation and growth kinetics.

Molecular beam epitaxy (MBE)

MBE enables atomically precise growth under ultra-high vacuum. Effusion cells supply elemental beams that condense epitaxially on heated substrates. While offering unparalleled control, MBE is costly and slow, used primarily for heterostructure research rather than mass production.

Atomic layer deposition (ALD) and plasma methods

ALD permits layer-by-layer deposition of oxides and nitrides with angstrom-scale control. Plasma-enhanced CVD (PECVD) lowers growth temperatures and tunes defect densities. These methods are suited for conformal coatings, encapsulation, and dielectric integration.

Solution and chemical synthesis

Graphene oxide (GO) is synthesized by oxidizing graphite via Hummers' method, yielding functionalized sheets dispersible in water. Reduction yields rGO with partial restoration of conductivity (Dreyer *et al.*, 2010). MXenes are derived by selective etching of A-layers from MAX phases using HF or in situ generated etchants (Naguib *et al.*, 2011). Surface terminations (–O, –OH, –F) critically influence electronic and interfacial properties (Anasori *et al.*, 2017).

Transfer and Integration

Large-area films often require transfer from growth substrates (Cu, Ni, sapphire) to target platforms (SiO_2/Si, glass, polymers). Wet transfer uses polymer supports (e.g., PMMA) followed by etching of growth substrates, introducing risks of contamination and wrinkles (Reina *et al.*, 2009). Dry transfer using thermal release tapes or lamination minimizes residues. Alignment for heterostructures (e.g., twisted bilayer graphene) demands sub-degree precision.

Equation (strain energy during transfer):

$$U = \tfrac{1}{2} \cdot E \cdot \varepsilon^2 \cdot V$$

Where:

U = elastic strain energy [J]
E = Young's modulus [Pa]
ε = strain
V = volume [m^3].

Managing strain reduces wrinkling and cracking.

Processing into Usable Forms

Inks and printing

Dispersions of graphene, MXenes, and TMDs are formulated into inks for inkjet, aerosol-jet, and screen printing. Rheology (viscosity η, surface tension γ) must be tuned for nozzle stability and film uniformity (Secor *et al.*, 2015).

Films and laminates

Vacuum filtration assembles nanosheets into freestanding membranes. Spray coating, spin coating, and blade coating enable scalable films with tunable thickness. Post-deposition annealing reduces defects and restores conductivity.

Composites

2D materials disperse into polymer, metal, or ceramic matrices to enhance mechanical, thermal, and electrical properties. Achieving uniform dispersion and interfacial bonding is key to performance.

Comparative Overview

Table 2 summarizes synthesis routes, highlighting scale, quality, and integration suitability.

Exfoliation routes provide accessible quantities but limited control, while CVD and MBE yield high-quality films at higher cost. Chemical synthesis (GO, MXenes) bridges scalability and functionality but requires surface control.

Table 2: Synthesis route pros/cons vs. KPIs

Method	Scale	Quality	Cost	Applications
Mechanical exfoliation	μm flakes, low yield	Defect-free	Low	Research, prototypes
LPE	g-scale dispersions	Small, defective flakes	Moderate	Inks, composites
Electrochemical exfoliation	g-scale	Residues, controllable	Moderate	Graphene, MXene precursors
CVD	Wafer-scale	Good, domain boundaries	High	Transparent conductors, electronics
MBE	cm^2	Excellent	Very high	Research heterostructures
ALD/PECVD	cm^2	Tunable	High	Dielectrics, coatings
GO synthesis	g-kg scale	Defective, functionalized	Low	Membranes, composites
MXene etching	g-scale	Metallic, surface terminations	Moderate	EMI, energy storage

Conclusion

Synthesis and processing routes dictate the balance between quality, scalability, and cost in 2D material applications. Mechanical exfoliation remains indispensable for benchmark studies, while liquid-phase and electrochemical exfoliation supply inks and composites.

Chemical vapor deposition delivers wafer-scale films for transparent conductors and electronics, whereas atomic layer and plasma processes integrate functional oxides and dielectrics. Chemical syntheses yield functionalized families such as GO and MXenes, expanding the property palette but introducing stability and contamination considerations.

Transfer methods and processing into inks, films, and composites complete the pipeline from atomic sheets to usable engineering forms. The choice of route is inherently application-specific, requiring engineers to weigh defect tolerance, lateral size, throughput, and integration compatibility.

Chapter 3: Structure–Property–Performance & Characterization of Two-Dimensional Materials

Understanding the linkage between structure, properties, and performance is central to engineering with two-dimensional (2D) materials. Their reduced dimensionality introduces unique phenomena such as tunable bandgaps, strong excitonic effects, and extreme anisotropy in thermal and mechanical behavior.

Engineering practice requires reliable characterization to correlate these structural features with functional properties and, ultimately, with device and system performance. This chapter reviews the structure–property relationships in 2D materials and outlines the characterization techniques that allow engineers to extract relevant parameters for design and quality assurance.

Electronic and Optical Structure

Band structure fundamentals

Graphene's linear dispersion relation at the Dirac points is expressed as:

$$E(\mathbf{k}) = \hbar v_F |\mathbf{k}|$$

Key:

E = energy [J]
$\mathbf{k}$ = wavevector [m^{-1}]
$\hbar$ = reduced Planck constant [J·s]
v_F = Fermi velocity [$m \cdot s^{-1}$].

This leads to massless Dirac fermion behavior, high carrier mobility, and ambipolar conduction (Novoselov *et al.*, 2005).

Transition-metal dichalcogenides (TMDs) such as MoS_2 exhibit a transition from indirect to direct bandgap at monolayer thickness (~1.8 eV). The strong excitonic effects result in sharp photoluminescence peaks with binding energies on the order of hundreds of meV (Mak *et al.*, 2010). Such features make TMDs suitable for optoelectronics and valleytronic applications (Xiao *et al.*, 2012).

Phosphorene shows a thickness-dependent direct bandgap ranging from ~0.3 eV (bulk) to ~2 eV (monolayer), with anisotropic effective masses along armchair and zigzag directions, influencing mobility and optical absorption (Li *et al.*, 2014).

Optical absorption and emission

Optical absorption spectra are dominated by excitonic resonances in TMDs, while graphene exhibits universal optical conductivity with absorption ~πα ≈ 2.3% per monolayer, where α is the fine-structure constant (Nair *et al.*, 2008). This property underpins graphene's use in transparent conductors.

Thermal Properties

Graphene exhibits extraordinary in-plane thermal conductivity (>2000 $W \cdot m^{-1} \cdot K^{-1}$) driven by long phonon mean free paths (Balandin, 2011). TMDs and phosphorene show significantly lower conductivities (~30–80 $W \cdot m^{-1} \cdot K^{-1}$) with anisotropy. Out-of-plane thermal conductivity is generally two orders of magnitude lower, a crucial consideration for thermal interface materials.

Equation (Fourier's law for 2D slab):

$$q = -\, k_{2\mathrm{D}} A \frac{\Delta T}{L}$$

Key:

q = heat flow [W]
k_{2D} = in-plane thermal conductivity [$W \cdot m^{-1} \cdot K^{-1}$]
A = cross-sectional area [m^2]
ΔT = temperature difference [K]
L = length [m].

Mechanical Properties

Graphene's Young's modulus approaches 1 TPa, with intrinsic tensile strength ~130 GPa (Lee *et al.*, 2008). AFM nanoindentation of suspended membranes quantifies these values, revealing failure modes and defect influences. Phosphorene and TMDs have lower moduli (~100–300 GPa) but retain mechanical flexibility relevant for flexible electronics.

Equation (membrane bulge test):

$$\Delta p = \frac{4Et}{a^2}\ \varepsilon$$

Key:

Δp = pressure difference [Pa]
E = Young's modulus [Pa]
t = thickness [m]
a = membrane radius [m]
ε = strain.

This relation is applied in thin-film mechanical testing.

Surface and Interfacial Properties

Surface energy governs adhesion, wettability, and composite compatibility. Contact angle goniometry provides insights into hydrophobicity (graphene) versus hydrophilicity (GO, MXenes). Functional groups on GO or MXenes introduce tunability for composites, catalysis, and membranes (Dreyer *et al.*, 2010; Anasori *et al.*, 2017).

Characterization techniques

Raman and photoluminescence spectroscopy

Raman spectroscopy identifies layer number, defects, strain, and doping. For graphene, the G (~1580 cm^{-1}), 2D (~2700 cm^{-1}), and D (~1350 cm^{-1}) peaks provide a fingerprint (Ferrari and Basko, 2013). Intensity ratios (I_2D/IG, ID/IG) indicate layer number and disorder. In TMDs, Raman modes (E^2g and A1g) shift with thickness, while PL intensity rises sharply for monolayers.

Microscopy

Atomic force microscopy (AFM) measures thickness and surface roughness. Transmission electron microscopy (TEM) resolves atomic lattices, dislocations, and grain boundaries. Scanning tunneling microscopy (STM) and spectroscopy (STS) probe local density of states.

X-ray and photoelectron techniques

X-ray diffraction (XRD, GIWAXS) reveals stacking order and crystallinity. X-ray photoelectron spectroscopy (XPS) and ultraviolet photoelectron spectroscopy (UPS) determine chemical states and work function. These methods are critical for verifying GO functionalization and MXene surface terminations (Ling *et al.*, 2014).

Electrical and thermal measurements

Van der Pauw and Hall measurements extract carrier type, density, and mobility. Four-point probe methods yield sheet resistance (IEC TS 62607-6-7). Time-domain thermoreflectance (TDTR) and optothermal Raman quantify thermal conductivity (Cahill, 2004).

Equation (Hall mobility):

$$\mu = \frac{\sigma}{nq}$$

Key:

μ = mobility [$m^2 \cdot V^{-1} \cdot s^{-1}$]
σ = conductivity [$S \cdot m^{-1}$]
n = carrier density [m^{-3}]
q = elementary charge [C].

Structure–Property–Performance Correlations

Linking characterization to application is central to engineering design. For example, ID/IG ratios in Raman correlate with defect density, which impacts conductivity and mechanical integrity. PL intensity in TMDs signals direct-gap behavior critical for optoelectronics. XPS-derived oxygen content in GO predicts membrane permeability and composite bonding. Hall mobility measurements directly inform device speed in field-effect transistors.

Comparative Overview

Table 3 summarizes key properties of representative 2D materials. The comparison shows how electronic structure, mechanical stiffness, and thermal transport vary widely across families, guiding application fit.

Table 3: Characterization matrix of 2D materials

Material	Bandgap (eV)	Young's modulus (GPa)	Thermal conductivity ($W \cdot m^{-1} \cdot K^{-1}$)	Mobility ($cm^2 \cdot V^{-1} \cdot s^{-1}$)	References
Graphene	0	~1000	>2000	>10,000	(Novoselov *et al.*, 2005; Balandin, 2011)
MoS_2 (ML)	~1.8	~270	30–50	200	(Mak *et al.*, 2010; Radisavljevic *et al.*, 2011)
h-BN	~6	~800	~300	–	(Watanabe *et al.*, 2004)
Phosphorene	0.3–2	~100	20–40	1000	(Li *et al.*, 2014)
Ti_3C_2 MXene	Metallic	~500	~50	–	(Naguib *et al.*, 2011; Anasori *et al.*, 2017)

Conclusion

The interplay between structure and properties defines the engineering potential of 2D materials. Graphene exemplifies extreme in-plane transport and strength, while TMDs offer bandgaps suitable for electronics and optoelectronics. Phosphorene introduces anisotropic semiconducting behavior, and MXenes provide high conductivity with surface functional tunability. Reliable characterization tools, Raman, PL, AFM, TEM, XPS, Hall, and thermal probes, allow engineers to measure and control these features. By linking structure to performance, engineers can make informed choices for application-specific integration, ensuring that material selection and processing align with system-level performance requirements.

Chapter 4 : Manufacturing at Scale & Printing of Two-Dimensional Materials

The transition from laboratory prototypes to industrial products requires scalable manufacturing and robust quality assurance for two-dimensional (2D) materials. Engineers must understand how materials can be processed into films, coatings, and components with consistent properties across large areas.

This chapter explores large-scale production methods, formulation of inks and dispersions, deposition and printing techniques, roll-to-roll processes, and the associated quality control protocols. The emphasis is on how to balance throughput, cost, and performance, with practical metrics for engineers to adopt in procurement and specification.

Inks and Dispersions

Stabilization and rheology

Stable dispersions are essential for printing and coating. Colloidal stability depends on surface charge, steric hindrance, and solvent compatibility. The zeta potential (ζ) quantifies electrostatic repulsion; values $|\zeta| > 30$ mV typically indicate good stability (Hunter, 1981). Rheology governs printability: viscosity (η) and surface tension (γ) must fall within process windows. For inkjet printing, $\eta \approx$ 1–20 mPa·s and $\gamma \approx$ 25–40 mN·m^{-1} are typical ranges (Secor *et al.*, 2015).

Equation (dimensionless printability number):

$$Z = \frac{1}{Oh} = \frac{\sqrt{\rho\gamma a}}{\eta}$$

Key:

- Z = printability number
- Oh = Ohnesorge number
- ρ = density [kg·m^{-3}]
- γ = surface tension [N·m^{-1}]
- a = nozzle diameter [m]
- η = viscosity [Pa·s].

Printable inks usually require $1 < Z < 10$.

Formulation strategies

Graphene and MXene inks can be prepared from liquid-phase exfoliated dispersions or chemically synthesised materials (Coleman *et al.*, 2011; Anasori *et al.*, 2017). Additives such as polymers (e.g., PVP, PEDOT:PSS) improve film formation and adhesion. For GO, aqueous dispersions are stable due to oxygen functional groups, but reduction is necessary to restore conductivity (Dreyer *et al.*, 2010).

Printing and Coating Techniques

Inkjet and aerosol-jet printing

Inkjet printing deposits picolitre droplets under digital control, enabling fine features (<50 μm). It is suited for prototyping conductive traces and sensors but limited by nozzle clogging and throughput. Aerosol-jet printing extends resolution to ~10 μm using aerodynamic focusing, relevant for high-density interconnects (Secor *et al.*, 2015).

Screen, gravure, and flexographic printing

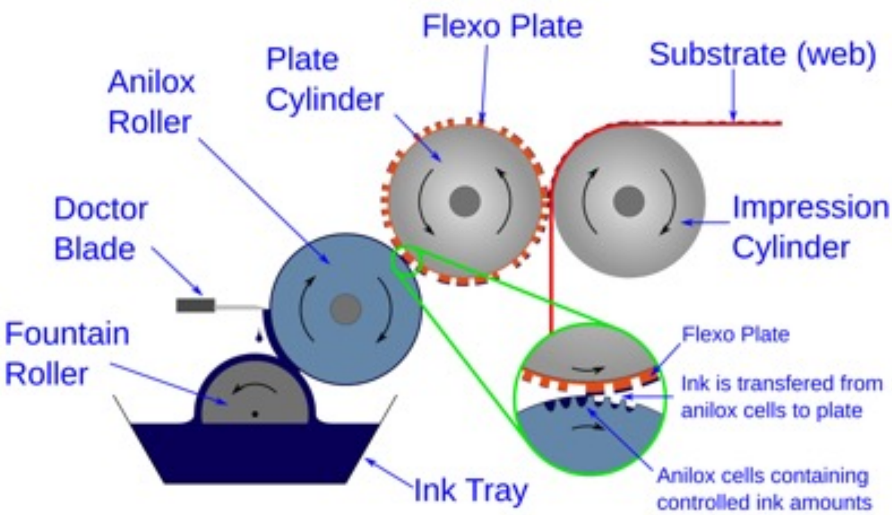

Figure 3: Typical flexographic printing apparatus

Credit: ECTran71, via Wikimedia Commons

These high-throughput methods, adapted from the graphics industry, process inks with higher viscosities and enable roll-to-roll manufacturing. Figure shows the general operating principle of a typical flexographic printing apparatus. Screen printing produces thicker, more conductive features (>10 μm), while gravure and flexographic printing offer continuous large-area coverage at web speeds >1 $m \cdot s^{-1}$.

Spray, spin, and blade coating

Spray coating is scalable for flexible substrates, spin coating yields uniform thin films but wastes material, and blade (doctor-blade, slot-die) coating is roll-to-roll compatible with precise thickness control (Kang *et al.*, 2012).

Equation (film thickness in slot-die coating):

$$h = \frac{Q}{\omega U}$$

Key:

h = film thickness [m]
Q = volumetric flow rate [$m^3 \cdot s^{-1}$]
ω = coating width [m]
U = substrate speed [$m \cdot s^{-1}$].

Roll-to-roll production

Roll-to-roll (R2R) processing integrates CVD growth, transfer, or printing into continuous lines. For graphene, Cu foils can be continuously fed through CVD furnaces and subsequently etched and transferred to polymer supports (Bae *et al.*, 2010). MXenes and GO can be processed from dispersions into continuous films using filtration or coating lines.

R2R methods address scalability but introduce challenges in uniformity, contamination, and mechanical defects. Inline monitoring (Raman mapping, sheet resistance measurement, optical inspection) is essential to maintain quality across kilometers of product.

Quality control and metrics

Electrical and optical benchmarks

A widely used performance metric for transparent conductors is the figure of merit (Haacke, 1976):

$$\Phi_{TC} = \frac{T^{10}}{R_s}$$

Key:

Φ_{TC} = figure of merit [Ω^{-1}]

T = transmittance at 550 nm

R_s = sheet resistance [Ω/sq].

High-performance films exhibit $\Phi_{TC} > 35 \times 10^{-3}\ \Omega^{-1}$.

Structural and chemical checks

- Raman spectroscopy: ID/IG ratio for defect density, $I_{2}D/IG$ for layer count (Ferrari and Basko, 2013).
- XPS: oxygen or termination content in GO/MXenes (Ling *et al.*, 2014).
- AFM/SEM: thickness and lateral uniformity.
- Contact angle: surface wettability for composite compatibility.

Reliability and yield

Mechanical robustness is tested by cyclic bending, adhesion tape tests, and thermal cycling. Yield maps of sheet resistance or Raman features identify defective regions.

Comparative Overview

Table 4 compares deposition methods by resolution, throughput, typical thickness, and industrial readiness. Inkjet and aerosol-jet excel in precision but are slow, while screen, gravure, and slot-die provide industrial scalability with trade-offs in resolution.

Table 4: Deposition and printing techniques

Method	Resolution	Throughput	Thickness	Industrial readiness
Inkjet	20–50 μm	Low	<1 μm	Prototyping
Aerosol-jet	~10 μm	Low–medium	<1 μm	Flexible electronics
Screen	>50 μm	High	1–20 μm	Mature
Gravure/flexographic	20–100 μm	Very high	0.1–5 μm	Mature, R2R
Slot-die/blade	10–100 μm	High	0.05–5 μm	Mature, R2R

Conclusion

Scalable manufacturing of 2D materials hinges on stable dispersions, compatible printing or coating processes, and rigorous quality control. Inkjet and aerosol-jet printing support rapid prototyping, whereas screen, gravure, and slot-die techniques underpin industrial-scale roll-to-roll production. Performance is evaluated using optical-electrical figures of merit, Raman/XPS metrics, and mechanical reliability tests.

Successful industrial adoption requires harmonizing ink formulation, deposition parameters, and inline monitoring, ensuring that 2D materials can transition from laboratory novelty to reliable components in commercial devices and systems.

Chapter 5: Devices & Systems I: Electrical, Optical, and EMI Applications of 2D Materials

Two-dimensional (2D) materials have attracted substantial attention for electrical, optical, and electromagnetic interference (EMI) applications due to their unique combination of conductivity, transparency, flexibility, and tunable optical responses. The ability to fabricate lightweight, flexible, and multifunctional devices using atomically thin materials offers clear advantages over conventional bulk systems.

This chapter explores the electrical and optical device landscape, emphasizing design considerations, governing relations, and real-world performance trade-offs relevant to engineers.

Transparent Conductors

Role and metrics

Transparent conductors are essential in displays, touch panels, solar cells, and smart windows. Indium tin oxide (ITO) dominates but suffers from brittleness and scarcity of indium. Graphene and other 2D materials offer flexible, potentially low-cost alternatives.

Equation (optical–electrical trade-off):

$$T(\lambda) = e^{-\alpha(\lambda)d}$$

Key:

$T(\lambda)$ = transmittance at wavelength λ
$\alpha(\lambda)$ = absorption coefficient [m^{-1}]
d = thickness [m].

This describes optical attenuation, with thinner films favoring transparency at the expense of sheet conductivity.

Sheet resistance relation:

$$R = R_s N$$

Key:

R total resistance [Ω]

R_s sheet resistance [Ω/sq]

N number of squares.

Low R_s values are critical for efficient conductors.

Graphene monolayers exhibit ~97.7% transparency (Nair *et al.*, 2008) but Rs typically >500 Ω/sq. Layer stacking, chemical doping, and hybridization with metallic nanowires improve conductivity while retaining transparency (Bonaccorso *et al.*, 2010).

Figures of merit

Haacke's figure of merit (Φ_{TC}) balances transparency and sheet resistance (Haacke, 1976):

$$\Phi_{TC} = \frac{T^{10}}{R_s}$$

Key:

Φ_{TC} = transparent conductor figure of merit [Ω^{-1}]

T = optical transmittance at 550 nm

R_s = sheet resistance [Ω/sq].

High-performance 2D films report Φ_{TC} values approaching those of ITO (>35 × 10^{-3} Ω^{-1}).

Flexible Heaters

Graphene and MXene films can be engineered as transparent, flexible heaters for de-icing, medical patches, or automobile defogging.

Joule heating follows:

$$P = I^2R = \frac{V^2}{R}$$

Key:

P = power [W]
I = current [A]
R = resistance [Ω]
V = voltage [V].

Design note:

Engineers must balance uniform heating with electrical safety. Rs uniformity across the film ensures consistent temperature distribution. MXene films have demonstrated rapid heating (>100 °C within seconds) under low voltages (Ling *et al.*, 2014).

Photodetectors and Optoelectronics

Photodetector fundamentals

Monolayer MoS_2 and other TMDs exhibit strong light–matter interactions due to direct bandgaps and large exciton binding energies. Responsivity (R) is defined as:

$$R = \frac{I_{ph}}{P_{opt}}$$

Key:

R = responsivity [$A \cdot W^{-1}$]
I_{ph} = photocurrent [A]
P_{opt} = incident optical power [W].

TMD photodetectors achieve responsivities up to ~880 $A \cdot W^{-1}$ under certain conditions (Lopez-Sanchez *et al.*, 2013). Heterostructures with graphene improve speed due to high carrier mobility.

Light-emitting devices

Heterostructures of graphene, h-BN, and TMDs enable LEDs and lasers. Radiative recombination in direct-gap TMDs allows for ultrathin light sources. Integration requires careful control of excitonic recombination zones.

EMI Shielding and Antennas

EMI shielding principles

Electromagnetic shielding effectiveness (SE) combines reflection, absorption, and multiple reflections:

$$SE_{total} = SE_R + SE_A + SE_M$$

Key:

SE_{total} = total shielding effectiveness [dB]

SE_R = reflection [dB]

SE_A = absorption [dB]

SE_M = multiple reflections [dB].

For conductive 2D films, absorption dominates at higher frequencies. Skin depth (δ) governs penetration:

$$\delta = \sqrt{\frac{2}{\omega\mu\sigma}}$$

Key:

δ = skin depth [m]

ω = angular frequency [$rad \cdot s^{-1}$]

μ = permeability [$H \cdot m^{-1}$]

σ = conductivity [$S \cdot m^{-1}$].

MXene films with conductivity >10^4 $S \cdot cm^{-1}$ demonstrate SE >50 dB at GHz frequencies at thicknesses <45 μm (Zhou *et al.*, 2019).

Antenna applications

Graphene and MXene conductors serve in lightweight antennas. The key metric is radiation efficiency, which depends on sheet conductivity and geometry. Graphene patch antennas achieve miniaturization but face challenges in high-frequency losses compared to metals (Tamagnone *et al.*, 2012).

Case studies

Case 1: Graphene Transparent Heater (Kang *et al.*, 2011)

Demonstrated as a defogging layer in automobile windshields, achieving rapid heating with Rs ~30 Ω/sq after chemical doping.

Background: Transparent heaters are widely used for defogging and de-icing in automotive and aerospace systems. Conventional heaters rely on ITO films, which are brittle and prone to failure under repeated bending.

Outcome: A graphene-based heater with sheet resistance of \~30 Ω/sq and optical transmittance above 90% was fabricated. The film achieved rapid heating to >100 °C within seconds at low voltages.

Lessons learnt: Graphene films provide flexibility and durability lacking in ITO, but uniform doping and encapsulation are essential to ensure consistent resistance and stable performance under cyclic bending.

Case 2: MXene EMI Shielding Films (Zhou *et al.*, 2019)

$Ti_3C_2T_x$ MXene papers achieved SE ~57 dB at 8–12 GHz with lightweight films, offering superior performance compared to conventional carbon composites.

Background: Aerospace requires lightweight EMI shielding to protect avionics and communication systems.

Outcome: Pilot-scale MXene films demonstrated SE >50 dB in GHz ranges, attracting interest for aerospace integration.

Lessons learnt: MXenes show high promise for EMI shielding markets, but industrial adoption depends on standardized datasheets, reproducibility, and long-term stability.

Case 3: TMD Photodetectors (Lopez-Sanchez *et al.*, 2013)

Achieved ultrahigh responsivity using hybrid structures with graphene electrodes, illustrating synergistic material integration.

Background: Infrared photodetection is vital for defense, sensing, and communications. Existing devices often require cooling or thick films.

Outcome: TMD-based photodetectors achieved high responsivity in ultrathin films, showing potential for miniaturized IR devices.

Lessons learnt: TMDs may disrupt optoelectronic markets, but scale-up and integration with existing device architectures remain challenges.

Comparative Overview

Table 5 summarizes representative electrical and optical device applications. 2D materials enable transparent, flexible conductors, highly sensitive photodetectors, and lightweight EMI shields. Performance hinges on balancing conductivity, optical transparency, frequency response, and stability.

Table 5: Electrical and optical device applications of 2D materials

Application	2D material	Key parameter	Typical performance	Reference
Transparent conductor	Graphene	R_s ~30 Ω/sq, T >90%	$\Phi_{TC} > 35\times10^{-3}\ \Omega^{-1}$	Kang *et al.*, 2011
Flexible heater	MXene film	Ramp rate	>100 °C in <30 s at <5 V	Ling *et al.*, 2014
Photodetector	MoS_2	Responsivity	~880 $A\cdot W^{-1}$	Lopez-Sanchez *et al.*, 2013
EMI shielding	MXene	SE	>50 dB @ GHz	Zhou *et al.*, 2019

Conclusion

2D materials offer unique opportunities for transparent conductors, heaters, photodetectors, and EMI shielding components. Key governing relations, optical absorption, sheet resistance, Joule heating, responsivity, and skin depth, allow engineers to predict device behavior and design accordingly.

While graphene excels in transparency and mobility, TMDs contribute direct bandgaps for optoelectronics, and MXenes provide outstanding EMI shielding. Careful consideration of material properties, fabrication strategies, and trade-offs enables deployment in real-world systems where flexibility, weight, and multifunctionality are paramount.

Chapter 6: Devices & Systems II: Chemical, Energy, and Membrane Applications of 2D Materials

Two-dimensional (2D) materials extend their utility far beyond electronic and optical devices. Their high surface-to-volume ratio, tunable surface chemistry, and unique transport properties make them particularly promising for chemical sensors, electrochemical energy systems, and selective membranes.

This chapter explores how 2D materials function in chemical detection, batteries, supercapacitors, electrocatalysis, and molecular sieving membranes. Governing transport equations, performance metrics, and case studies are presented to provide engineers with the tools for design and evaluation.

Chemical Sensors

Sensing mechanisms

Graphene, TMDs, and MXenes serve as platforms for chemical and biological sensing due to strong adsorption–induced changes in conductivity and work function.

The fundamental sensing principle is:

$$\Delta R = S \cdot C$$

Key:

ΔR = change in resistance [Ω]
S = sensitivity constant [$\Omega \cdot (\mathrm{mol \cdot m^{-3}})^{-1}$]
C = analyte concentration [$\mathrm{mol \cdot m^{-3}}$].

In graphene, gas molecules such as NO_2 or NH_3 act as electron donors/acceptors, shifting the Fermi level (Schedin *et al.*, 2007). TMDs provide higher baseline resistance, yielding larger relative changes upon adsorption. MXenes, with their hydrophilic, functionalized surfaces, are effective for aqueous and biosensing applications (Sarycheva *et al.*, 2018).

Device configurations

Sensors are often fabricated as chemiresistors or field-effect transistors (FETs). In FET-based sensors, adsorbed molecules shift threshold voltage, altering channel current. Selectivity is enhanced by functionalization with polymers, nanoparticles, or biomolecules.

Electrochemical Energy Storage

Supercapacitors

Graphene and MXenes provide high specific surface areas (>1000 $m^2 \cdot g^{-1}$) and conductivity for double-layer capacitance. MXenes also contribute pseudocapacitance via redox-active terminations (Gogotsi and Anasori, 2019).

Equation (capacitance):

$$C = \frac{\varepsilon A}{d}$$

Key:

C = capacitance [F]
ε = permittivity [$F \cdot m^{-1}$]
A = electrode area [m^2]
d = effective separation distance [m].

Energy density (E) scales as:

$$E = ½\, CV^2$$

Key:

E = energy density [J]
C = capacitance [F]
V = voltage [V].

Graphene supercapacitors typically reach energy densities of ~5 $Wh \cdot kg^{-1}$, whereas MXene-based systems exceed 20 $Wh \cdot kg^{-1}$ while maintaining high power density (Lukatskaya *et al.*, 2013).

Batteries

Phosphorene, TMDs, and MXenes act as anodes or cathodes in Li-ion, Na-ion, and K-ion batteries.

Ion intercalation is governed by diffusion:

$$J = -D\frac{\Delta C}{\Delta x}$$

Key:

J = flux [mol·m^{-2}·s^{-1}]
D = diffusion coefficient [m^2·s^{-1}]
ΔC = concentration gradient [mol·m^{-3}]
Δx = diffusion length [m].

MXenes provide high-rate capabilities due to metallic conductivity and short diffusion paths, achieving >400 mAh·g^{-1} capacities (Xie *et al.*, 2014).

Electrocatalysis

2D materials serve as electrocatalysts for hydrogen evolution (HER), oxygen evolution (OER), and oxygen reduction (ORR). Catalytic activity depends on active sites and binding energies. TMDs such as MoS_2 are prototypical HER catalysts, with activity concentrated at edges (Jaramillo *et al.*, 2007).

The Butler–Volmer relation describes electrode kinetics:

$$i = i_0\left[e^{anF\eta/RT} - e^{-(1-a)nF\eta/RT}\right]$$

Key:

i = current density [A·m^{-2}]
i_0 = exchange current density [A·m^{-2}]
α = charge transfer coefficient
n = number of electrons
F = Faraday constant [C·mol^{-1}]
η = overpotential [V]
R = gas constant [J·mol^{-1}·K^{-1}]
T = temperature [K].

MXenes and doped graphene derivatives have been engineered to improve catalytic performance through electronic structure tuning and defect creation.

Membranes and Molecular Sieving

Graphene oxide membranes

Graphene oxide (GO) laminates allow water permeation while blocking larger solutes (Nair *et al.*, 2012). Interlayer spacing, controlled by functionalization or cross-linking, defines selectivity.

Equation (permeance):

$$P = \frac{J}{\Delta p}$$

Key:

P = permeance [mol·m^{-2}·s^{-1}·Pa^{-1}]
J = flux [mol·m^{-2}·s^{-1}]
Δp = pressure difference [Pa].

Ion-selective and gas-separation membranes

MXene and TMD membranes demonstrate ion sieving for desalination and energy applications. Control of thickness, pore size, and functionalization governs separation performance. Phosphorene-based membranes show anisotropic transport promising for niche separation tasks (Sun *et al.*, 2017).

Case studies

Case 1: Graphene NO_2 Sensor (Schedin *et al.*, 2007)

Detection down to single molecules via resistance shifts.

Background: Detecting low concentrations of toxic gases such as NO_2 is vital for environmental monitoring and workplace safety.

Outcome: Graphene sensors achieved single-molecule detection sensitivity by monitoring resistance changes. Adsorbed molecules shifted the Fermi level, producing clear, measurable signals.

Lessons learnt: Graphene's high surface-to-volume ratio provides extraordinary sensitivity. Selectivity remains a challenge, requiring functionalization strategies to target specific gases.

Case 2: MXene Supercapacitor (Lukatskaya *et al.*, 2013)

Volumetric capacitance >1500 F·cm^{-3} with stable cycling.

Background: High-power energy storage devices are critical for grid balancing and electric vehicles. Supercapacitors trade energy density for rapid charging/discharging.

Outcome: $Ti_3C_2T_x$ MXene films achieved volumetric capacitances >1500 F·cm^{-3}, with stable cycling over thousands of charge–discharge cycles.

Lessons learnt: MXenes bridge the gap between capacitors and batteries by offering high capacitance and good cycling stability. However, scalability and oxidation resistance are barriers for commercialization.

Case 3: MoS_2 HER Catalyst (Jaramillo *et al.*, 2007)

Comparable activity to noble metals when edge sites are maximized.

Background: Hydrogen evolution reaction (HER) is central to green hydrogen production. Platinum is the benchmark catalyst but is costly and scarce.

Outcome: MoS_2 catalysts exhibited high HER activity, with edge sites providing catalytic activity comparable to Pt. Basal planes remained largely inert.

Lessons learnt: Engineering defects and increasing edge density dramatically improve catalytic activity. This case highlights the importance of nanoscale morphology in determining catalytic efficiency.

Case 4: GO Desalination Membrane (Nair *et al.*, 2012)

High water flux with NaCl rejection ~97%.

Background: Desalination technologies are essential for addressing global water scarcity, but conventional membranes are energy-intensive and limited in selectivity.

Outcome: GO laminates allowed water molecules to pass while rejecting NaCl with ~97% efficiency, demonstrating both high flux and selectivity.

Lessons learnt: GO membranes offer a pathway to energy-efficient desalination. However, long-term stability in saline environments and fouling resistance require further development.

Comparative Overview

Table 6 summarizes representative energy and chemical applications. 2D materials offer ultra-sensitive sensors, high-capacity electrodes, efficient electrocatalysts, and selective membranes. Each application exploits structural features such as surface chemistry, layer spacing, and conductivity.

Table 6: Energy and chemical applications of 2D materials

Application	Material	Metric	Typical performance	Reference
Gas sensor	Graphene	Detection limit	Single molecules	Schedin *et al.*, 2007
Supercapacitor	MXene	Energy density	~20 Wh·kg^{-1}	Lukatskaya *et al.*, 2013
Battery anode	MXene	Capacity	>400 mAh·g^{-1}	Xie *et al.*, 2014
HER catalyst	MoS_2	Exchange current density	Comparable to Pt edges	Jaramillo *et al.*, 2007
GO membrane	GO	NaCl rejection	~97%	Nair *et al.*, 2012

Conclusion

The chemical, energy, and membrane applications of 2D materials showcase their capacity to transform sectors beyond electronics. Graphene and TMDs enable highly sensitive chemical detection, MXenes provide both energy storage and catalytic activity, and GO membranes demonstrate remarkable selectivity in separations.

Governing relations for adsorption, diffusion, capacitance, and electrocatalysis provide engineers with predictive tools. With continued advances in stability, integration, and scalability, 2D materials are poised to become integral in next-generation energy systems and filtration technologies.

Chapter 7: Composites, Coatings & Tribology with 2D Materials

Two-dimensional (2D) materials have been widely explored as reinforcement agents in composites, as barrier and protective coatings, and as solid lubricants in tribological systems. Their large aspect ratio, high stiffness, tunable surface chemistry, and inherent anisotropy create opportunities to enhance mechanical, thermal, electrical, and chemical performance of bulk materials.

This chapter examines how 2D materials are integrated into composites and coatings, the governing models that describe property enhancements, and their tribological applications in reducing wear and friction.

Composites

Role of 2D fillers

Graphene, MXenes, h-BN, and transition-metal dichalcogenides (TMDs) act as multifunctional fillers in polymer, metal, and ceramic matrices. Their high aspect ratios promote percolation at low loadings, enabling conductivity and reinforcement without significant density increases (Potts *et al.*, 2011). Achieving uniform dispersion and strong interfacial bonding is critical; otherwise, aggregation or weak adhesion undermines reinforcement.

Mechanical reinforcement

The Halpin–Tsai model predicts effective modulus (E_c) of composites:

$$E_c = E_m \frac{1 + \xi \eta \Phi}{1 - \eta \Phi}$$

Where:

$$E_c = E_m \frac{1 + \xi \eta \Phi}{1 - \eta \Phi}$$

Key:

E_c = composite modulus [Pa]

E_m = matrix modulus [Pa]

E_f = filler modulus [Pa]
φ = filler volume fraction
ξ = shape factor dependent on aspect ratio.

Graphene's modulus (~1 TPa) significantly enhances stiffness even at φ <1%, provided dispersion and alignment are adequate (Young *et al.*, 2012).

Electrical and thermal percolation

The percolation threshold (φ_c) defines the filler loading at which conductive networks form:

$$\sigma = \sigma_0(\phi - \phi_c)^t$$

Key:

σ = composite conductivity [S·m^{-1}]
σ_0 = scaling factor [S·m^{-1}]
φ = filler volume fraction
φ_c = critical filler fraction
t = critical exponent (~1.3–2.0).

Graphene–polymer composites exhibit φ_c values <0.5 vol%, much lower than carbon black, making them attractive for antistatic and EMI shielding applications (Stankovich *et al.*, 2006).

Thermal transport

Effective thermal conductivity can be estimated using the Maxwell–Eucken relation:

$$k_{eff} = k_m \frac{k_f + 2k_m - 2\phi(k_m - k_f)}{k_f + 2k_m + \phi(k_m - k_f)}$$

Key:

k_{eff} = effective conductivity [W·m^{-1}·K^{-1}]
k_m= matrix conductivity [W·m^{-1}·K^{-1}]
k_f = filler conductivity [W·m^{-1}·K^{-1}]
φ = volume fraction.

Graphene and BN nanosheets significantly increase thermal conductivity of polymers, enhancing their role as thermal interface materials (Yu *et al.*, 2008).

Coatings

Barrier coatings

Graphene oxide (GO) laminates act as impermeable barriers, extending corrosion resistance of metals by creating tortuous diffusion pathways.

The tortuosity factor (τ) modifies Fick's law:

$$J = D_{eff}\,\frac{\Delta C}{\Delta x}, \quad D_{eff} = \frac{D}{\tau}$$

Key:

J + flux [mol·m^{-2}·s^{-1}]
D = diffusion coefficient [m^{2}·s^{-1}]
D_{eff} = effective diffusion coefficient [m^{2}·s^{-1}]
ΔC = concentration gradient [mol·m^{-3}]
Δx = thickness [m]
τ = tortuosity factor.

Corrosion tests show GO coatings extend salt spray resistance by >1000 h compared to uncoated steel (Chen *et al.*, 2012).

Functional and conductive coatings

MXene and graphene films serve as EMI shielding coatings on lightweight polymer substrates. Conductive coatings with Rs <20 Ω/□ and shielding effectiveness >40 dB at GHz frequencies have been demonstrated (Zhou *et al.*, 2019).

Protective coatings

h-BN coatings resist oxidation and provide dielectric protection at high temperatures (>900 °C). TMD coatings (e.g., MoS_2) act as solid lubricants in aerospace and mechanical systems.

Tribology

Solid lubrication

Layered 2D materials such as graphene, h-BN, and MoS_2 exhibit easy shear along basal planes due to weak interlayer van der Waals forces. This reduces friction coefficients (μ) to <0.05 under certain conditions (Berman *et al.*, 2015).

Wear resistance

Incorporating 2D nanosheets into lubricating oils or polymer matrices reduces wear by forming protective tribofilms at contact interfaces. These films limit direct asperity contact, decreasing material loss.

Equation (friction coefficient):

$$\mu = \frac{F_f}{F_N}$$

Key:

μ = coefficient of friction
F_f = friction force [N]
F_N normal force [N].

Applications

MoS_2-based lubricants are used in aerospace and vacuum systems, while graphene-enhanced oils improve engine durability. MXene additives are emerging for high-load lubrication due to metallic conductivity and surface functional groups (Zhao *et al.*, 2019).

Case studies

Case 1: Graphene–Epoxy Composite (Young *et al.*, 2012)

Enhanced tensile strength by ~40% at <0.1 wt% loading.

Background: Epoxy resins are widely used structural materials in aerospace, automotive, and civil engineering. Reinforcement with fillers improves strength and toughness.

Outcome: Addition of <0.1 wt% graphene increased tensile strength by ~40%. Improvements were attributed to effective load transfer across the graphene–matrix interface.

Lessons learnt: Even small amounts of graphene can dramatically enhance mechanical properties. Proper dispersion and interfacial adhesion are crucial to avoid aggregation that undermines reinforcement.

Case 2: GO Anticorrosion Coating (Chen *et al.*, 2012)

Extended steel corrosion resistance in saline environments by >1000 h.

Background: Corrosion of metals leads to significant maintenance costs in infrastructure and transportation sectors.

Outcome: GO coatings on steel extended salt spray resistance beyond 1000 h compared to uncoated controls. The laminated structure created a tortuous path for ion diffusion.

Lessons learnt: GO coatings provide excellent corrosion resistance through physical barrier effects. However, defects or pinholes can undermine performance, highlighting the need for uniform deposition.

Case 3: MoS_2 Aerospace Lubricant (Berman *et al.*, 2015)

Reliable low-friction operation under vacuum and high load.

Background: Aerospace and vacuum systems require lubricants that remain effective in extreme environments where oils volatilize.

Outcome: MoS_2 coatings delivered stable lubrication with coefficients of friction <0.05 in vacuum and high-load conditions.

Lessons learnt: Layered TMDs act as solid lubricants due to their easy-shear basal planes. Performance depends on maintaining crystalline order and avoiding oxidation.

Comparative Overview

Table 7 summarizes representative applications of composites, coatings, and tribological systems. 2D materials improve stiffness, conductivity, barrier properties, and tribological performance. The key lies in dispersion, adhesion, and interface design.

Table 7: Applications of composites, coatings, and tribological systems

Application	Material	Key metric	Performance	Reference
Polymer composite	Graphene	Modulus	+40% at 0.1 wt%	Young *et al.*, 2012
Barrier coating	GO	Salt spray resistance	>1000 h	Chen *et al.*, 2012
EMI coating	MXene	SE	>40 dB @ GHz	Zhou *et al.*, 2019
Solid lubricant	MoS_2	μ	<0.05	Berman *et al.*, 2015

Conclusion

2D materials substantially enhance the properties of composites, coatings, and lubricants. Their high aspect ratios, anisotropy, and tunable surface chemistry underpin advances in mechanical reinforcement, thermal conductivity, corrosion resistance, EMI shielding, and tribological performance.

Predictive models such as Halpin–Tsai, percolation theory, Maxwell–Eucken, and diffusion tortuosity guide engineering design. With proper dispersion and interface engineering, even small filler fractions achieve outsized effects, positioning 2D materials as powerful multifunctional additives in industrial applications.

Chapter 8: Reliability, EHS, and Lifecycle Considerations of 2D Materials

For 2D materials to transition from laboratory demonstrations to industrial deployment, engineers must consider reliability, environmental health and safety (EHS), and lifecycle impacts. These factors determine whether devices meet regulatory standards, maintain performance over years of use, and avoid unintended consequences for workers, users, and the environment.

This chapter examines degradation mechanisms, reliability testing, occupational exposure concerns, and end-of-life management of 2D materials.

Reliability in Devices

Electrical reliability

Conductive films such as graphene and MXenes are subject to drift in sheet resistance (Rs) due to oxidation, contamination, or moisture uptake. Accelerated stress testing involves applying current densities above operational levels to identify failure modes.

Equation (electromigration lifetime, Black's law):

$$t_f = AJ^{-n}e^{E_a/k_B T}$$

Key:

- t_f = time to failure [s]
- A = empirical constant
- J = current density [A·m^{-2}]
- n = scaling exponent (≈2)
- E_a = activation energy [eV]
- k_B = Boltzmann constant [eV·K^{-1}]
- T = temperature [K].

MXene films, though highly conductive, can oxidize under ambient humidity, reducing conductivity within weeks unless encapsulated (Zhou *et al.*, 2019).

Mechanical reliability

Flexing and bending can lead to crack propagation in 2D films. Bending radius tests quantify durability for flexible electronics. Fatigue life is related to strain amplitude (ε_a):

$$N_f = C \cdot \varepsilon_a^{-m}$$

Key:

N_f = cycles to failure
C, m = material constants
ε_a = strain amplitude.

Thermal and environmental reliability

High temperatures induce desorption of functional groups (e.g., oxygen from GO). UV irradiation accelerates degradation in polymers containing 2D fillers. Encapsulation strategies mitigate these effects.

Environmental Health and Safety (EHS)

Occupational exposure

Inhalation of nanosheets during synthesis or processing presents risks analogous to other nanomaterials. Graphene and GO powders can cause pulmonary inflammation in rodents (Schinwald *et al.*, 2012). MXenes generate acidic etching by-products (HF, LiF), requiring strict fume hood and PPE protocols (Anasori *et al.*, 2017).

Airborne nanosheets are characterized by aerodynamic diameter (d_a), influencing lung deposition:

$$d_a = d_p \sqrt{\rho_p / \rho_0}$$

Key:

d_a = aerodynamic diameter [m]
d_p = physical particle diameter [m]
ρ_p = particle density [$kg \cdot m^{-3}$]
ρ_0 = unit density (1000 $kg \cdot m^{-3}$).

Toxicological considerations

Surface chemistry influences biological responses. Hydrophilic GO tends to disperse in aqueous environments, whereas hydrophobic graphene aggregates. Functionalization can reduce cytotoxicity by improving biocompatibility (Seabra *et al.*, 2014).

Regulatory landscape

ISO/TS 80004-13 defines vocabulary for graphene and 2D materials, while OECD provides nanosafety testing guidelines. In the EU, REACH registration is mandatory for chemicals at scale, including nanomaterials. The US EPA has oversight under TSCA. These frameworks increasingly require lifecycle data for risk assessment.

Lifecycle assessment (LCA)

Production impacts

CVD graphene production is energy-intensive, with high-temperature furnaces operating at >1000 °C. Chemical synthesis routes (e.g., Hummers' method for GO) use strong oxidizers ($KMnO_4$, H_2SO_4), raising concerns about waste management and effluents (Dreyer *et al.*, 2010).

Use phase

Durability and stability influence environmental footprint. For instance, stable graphene-based coatings extend lifetime of metals, reducing replacement cycles and overall impact.

End-of-life

Few recycling methods exist for 2D materials. Potential strategies include thermal recovery, solvent dissolution, and re-dispersion for reuse in composites. Incineration risks releasing nanoparticles, so controlled disposal is advised.

Equation (impact factor in LCA):

$$IF = \sum_i E_i CF_i$$

Key:

IF = impact factor
E_i = emission of pollutant *i* [kg]
CF_i = characterization factor [impact units·kg^{-1}].

Case studies

Case 1: Graphene Film Reliability (Kim *et al.*, 2011)

Sheet resistance doubled after 1000 bending cycles at 1 mm radius unless encapsulated.

Background: Flexible electronics demand materials that withstand repeated bending without performance loss.

Outcome: Graphene conductive films doubled their sheet resistance after 1000 bending cycles at a 1 mm radius. Encapsulation stabilized performance by preventing crack propagation.

Lessons learnt: Mechanical durability is a key challenge for 2D materials. Encapsulation and substrate engineering mitigate degradation under repeated strain.

Case 2: MXene Oxidation Stability (Zhou *et al.*, 2019)

$Ti_3C_2T_x$ lost ~50% conductivity after 2 weeks in ambient humidity, mitigated by vacuum storage.

Background: MXenes offer high conductivity and surface tunability but degrade under ambient humidity.

Outcome: $Ti_3C_2T_x$ films lost ~50% conductivity after 2 weeks in air. Storage under vacuum or inert atmosphere preserved properties.

Lessons learnt: Environmental stability is critical for real-world adoption. Packaging and storage conditions must be designed into product lifecycles.

Case 3: GO Cytotoxicity and Biocompatibility (Seabra *et al.*, 2014)

Surface functionalization reduced oxidative stress in cell cultures.

Background: Health impacts of engineered nanomaterials are a regulatory and ethical concern.

Outcome: Functionalized GO reduced oxidative stress and cytotoxicity in cell cultures compared to pristine GO.

Lessons learnt: Surface functionalization can reduce toxicological risks and improve biocompatibility. Safety-by-design approaches are essential in nanomaterial development.

Comparative Overview

Table 8 summarizes reliability, EHS, and lifecycle issues. Reliability issues stem from environmental instability, EHS risks from inhalation and toxic by-products, and lifecycle concerns from synthesis impacts and disposal challenges. Mitigation involves encapsulation, PPE, greener chemistry, and recycling strategies.

Table 8: Reliability, EHS, and lifecycle issues

Category	Material	Key issue	Mitigation	Reference
Electrical reliability	MXene	Oxidation	Encapsulation, inert storage	Zhou *et al.*, 2019
Mechanical reliability	Graphene	Cracking under flexing	Substrate adhesion, encapsulation	Kim *et al.*, 2011
Occupational safety	GO	Pulmonary inflammation	PPE, fume hoods, dispersion control	Schinwald *et al.*, 2012
Lifecycle	GO	Hazardous synthesis	Greener oxidants, waste management	Dreyer *et al.*, 2010

Conclusion

The successful adoption of 2D materials in commercial products depends on ensuring long-term reliability, safeguarding worker and user health, and managing lifecycle impacts. Oxidation, cracking, and degradation are key reliability challenges, mitigated by encapsulation and interface engineering. EHS considerations highlight the importance of controlling exposure during synthesis and processing, with regulatory frameworks tightening oversight.

Lifecycle assessments reveal significant environmental burdens from energy-intensive synthesis and hazardous reagents, but also potential benefits from durability-enhancing applications. Addressing these challenges holistically will enable safe and sustainable integration of 2D materials in engineering practice.

Chapter 9: Standardization, Markets & Outlook for 2D Materials

The industrial adoption of two-dimensional (2D) materials depends not only on scientific breakthroughs but also on standardization, market development, and strategic forecasting. Engineers must navigate evolving international standards, understand the commercial landscape, and anticipate future directions for deployment.

This chapter reviews ongoing efforts in standardization, evaluates the market potential across sectors, and projects the near- and long-term outlook for 2D materials in engineering practice.

Standardization

Vocabulary and terminology

ISO/TS 80004-13 provides harmonized terminology for graphene and related 2D materials, including definitions for monolayer, few-layer, and multilayer materials, as well as flakes, films, and powders (ISO, 2024). This harmonization reduces ambiguity in technical specifications and facilitates cross-industry communication.

Measurement standards

The IEC has developed a suite of technical specifications (IEC TS 62607-6 series) to define **key control characteristics** for graphene-based materials. These cover sheet resistance (van der Pauw and four-point probe), defect density (Raman spectroscopy), functional groups (TGA–FTIR), and elemental composition (XPS) (IEC, 2022–2023). Comparable standards for MXenes and TMDs are under discussion.

Equation (IEC four-point probe relation):

$$R_s = \frac{\pi}{\ln 2} \cdot \frac{V}{I}$$

Key:

R_s = sheet resistance [Ω/sq]
V = voltage [V]
I = current [A].

Regulatory frameworks

The EU REACH framework requires registration of nanomaterials at commercial scale, while the US EPA regulates under TSCA. OECD nanosafety guidelines apply globally, shaping workplace practices. These frameworks demand traceability, hazard assessment, and safe handling protocols.

Market Landscape

Commercial sectors

Key sectors include:

- **Electronics:** flexible displays, transparent conductors, high-frequency devices.
- **Energy:** supercapacitors, batteries, fuel cells.
- **Membranes:** desalination, gas separation, biomedical filtration.
- **Composites:** structural reinforcement, EMI shielding, lightweight aerospace materials.

The **global graphene market** was valued at ~US$ 175 million in 2022, with a CAGR exceeding 35% projected for the next decade (IDTechEx, 2022). MXenes and TMDs are at earlier stages, but venture funding and pilot plants are accelerating.

Industrial readiness

Technology readiness levels (TRLs) vary: graphene composites (TRL 6–8) are entering commercial use, while TMD-based optoelectronics remain at TRL 3–4. MXenes are advancing rapidly in energy storage and EMI shielding but face stability hurdles.

Supply chain considerations

Challenges include:

- CVD scale-up costs for wafer-scale films.

- Environmental and safety impacts of chemical synthesis (e.g., GO, MXenes).
- Need for standardized datasheets to ensure comparability across suppliers.

Outlook and Trends

Technical trends

- **Heterostructures:** van der Waals stacking of graphene, h-BN, and TMDs for multifunctional devices (Geim and Grigorieva, 2013).
- **Quantum and neuromorphic devices:** exploiting 2D excitons and memristive behavior.
- **Green synthesis:** sustainable production methods to reduce lifecycle impacts.

Market drivers

- Push for flexible, wearable, and lightweight devices.
- Demand for high-performance batteries and supercapacitors in EVs.
- Global water scarcity driving desalination and purification membranes.
- Defense and aerospace adoption of EMI shielding composites.

Barriers and risks

- Material stability (oxidation of MXenes, degradation of phosphorene).
- Scale-up costs and variability in quality.
- Regulatory uncertainty regarding nanomaterial toxicity.

Case studies

Case 1: Graphene Composites in Sports Equipment (Graphene Flagship, 2020)

Commercial use in tennis rackets and helmets demonstrates mechanical reinforcement and branding appeal.

Background: Sports equipment companies are early adopters of advanced materials for performance and marketing differentiation.

Outcome: Graphene-enhanced tennis rackets and helmets were commercialized, with claims of improved stiffness and reduced weight.

Lessons learnt: Consumer products serve as testbeds for new materials, bridging the gap between laboratory validation and industrial adoption. Independent verification of performance claims remains essential.

Comparative Overview

Table 9 summarizes technology readiness and market status. Graphene leads in commercial adoption, MXenes are poised for rapid growth, while TMDs and phosphorene remain in early stages of technological development.

Table 9: Technology readiness and market status

Material family	Key applications	TRL range	Market status
Graphene	Composites, coatings, conductors	6–8	Entering mainstream
h-BN	Dielectrics, coatings	4–6	Niche markets
TMDs	Photodetectors, FETs	3–4	Research-focused
MXenes	Supercapacitors, EMI shielding	4–6	Pilot scale
Phosphorene	Photonics, sensors	2–3	Early-stage research

Conclusion

The future of 2D materials lies at the intersection of scientific progress, standardization, and market forces. Graphene has advanced furthest toward commercialization, with composites and coatings entering everyday products. MXenes show strong promise in EMI shielding and energy applications, pending stability improvements. TMDs and phosphorene remain research-intensive but hold potential for transformative optoelectronic and sensing technologies.

Standardization efforts by ISO and IEC are crucial for ensuring comparability and safety, while regulatory frameworks increasingly demand lifecycle transparency. With strong drivers in flexible electronics, clean energy, and water treatment, the outlook for 2D materials is positive, provided technical and regulatory challenges are met.

Chapter 10: Final Synthesis , Modern Materials: Two-Dimensional Materials

Course Overview

This course has provided a structured exploration of two-dimensional (2D) materials, from fundamental taxonomy to synthesis, properties, device integration, composites, and finally reliability, safety, and market outlook. Across nine modules, engineers are equipped with the theoretical foundations, quantitative models, characterization methods, and applied case studies necessary to understand and utilize 2D materials in professional practice.

Key Insights from the Modules

Foundations (Chapters 1–3)

- **Landscape and taxonomy:** 2D materials span graphene, h-BN, TMDs, phosphorene, and MXenes, each offering distinct electronic, thermal, and mechanical properties. Classification by bonding type, bandgap, and stability helps engineers match materials to applications.
- **Synthesis and processing:** Top-down (exfoliation, liquid-phase, electrochemical) and bottom-up (CVD, ALD, MBE, solution chemistry) methods trade off quality, scale, and cost. Processing into inks, films, and composites bridges laboratory materials and engineering components.
- **Structure–property–performance:** Raman spectroscopy, AFM, TEM, and electrical/thermal tests reveal the link between structure and functional properties. This enables engineers to validate vendor claims, ensure quality, and optimize device performance.

Devices and systems (Chapters 4–6)

- **Manufacturing at scale:** Printing and roll-to-roll coating enable industrial throughput. Figures of merit such as Haacke's Φ_{TC} guide evaluation of transparent conductors, while inline monitoring ensures uniformity.
- **Electrical, optical, and EMI applications:** Graphene supports transparent conductors and flexible heaters; TMDs offer photodetection and optoelectronic potential; MXenes excel in EMI shielding with conductivities rivaling metals.
- **Chemical, energy, and membranes:** Graphene and MXenes enable ultra-sensitive chemical sensing and supercapacitors; MoS_2 edges catalyze

hydrogen evolution; graphene oxide membranes demonstrate selective sieving, relevant for desalination.

Composite and lifecycle aspects (Chapters 7–9)

- **Composites, coatings, and tribology:** Even small fractions of 2D fillers reinforce mechanical, thermal, and barrier properties, guided by predictive models (Halpin–Tsai, percolation theory, Maxwell–Eucken). Coatings extend corrosion resistance, while solid lubricants reduce wear.
- **Reliability and EHS:** Degradation, oxidation, and cracking are reliability concerns; mitigation includes encapsulation and fatigue testing. EHS considerations highlight inhalation and toxicology risks, requiring PPE, greener synthesis, and regulatory compliance. Lifecycle assessments balance production impacts with durability gains.
- **Standardization and markets:** ISO and IEC standards underpin consistent terminology and measurement. Markets are expanding rapidly, with graphene composites entering commercial products, MXenes progressing in EMI shielding and energy, and TMDs advancing in optoelectronics. Regulatory oversight (REACH, EPA) ensures safety and lifecycle accountability.

Cross-cutting themes

- **Structure–processing–property link:** Success depends on controlling structure at atomic and mesoscale levels to deliver consistent macroscopic properties.
- **Scalability vs. quality:** Engineers must weigh the trade-offs between pristine lab samples and industrially viable materials.
- **Reliability and safety:** Long-term stability, occupational safety, and lifecycle impacts are integral to engineering decisions, not afterthoughts.
- **Interdisciplinarity:** Progress requires convergence of physics, chemistry, materials science, mechanical engineering, and regulatory policy.

Outlook

The outlook for 2D materials is highly positive, with strong drivers in flexible electronics, energy storage, water treatment, and aerospace composites. Standardization will reduce uncertainty and accelerate industrial adoption. Green synthesis and lifecycle transparency will address environmental concerns. Multifunctional heterostructures and emerging MXene-based systems promise disruptive applications. Engineers will play a key role in translating these materials from the laboratory to the marketplace, ensuring they are safe, reliable, and economically viable.

Final conclusion

Two-dimensional materials represent a new frontier in engineering materials, combining atomic-scale precision with macroscopic versatility. This course has the knowledge base to critically assess, design, and implement 2D materials in practice. By integrating scientific understanding with industrial pragmatism, engineers can harness the unique properties of 2D materials to address societal challenges in energy, environment, and technology, shaping the next generation of modern materials for a sustainable future.

Appendix A : Worked Examples of Key Formulae

This appendix provides worked numerical examples for the key formulae introduced throughout the course. Each example includes context for why the formula matters in engineering practice, calculation steps, and interpretation of what the result implies for material performance or design.

A1. Surface energy matching in liquid-phase exfoliation

Formula:

$$\gamma_s \approx \gamma_f$$

Context: Effective liquid-phase exfoliation of layered crystals requires solvents with surface energies close to the surface energy of the nanosheet. Mismatches lead to aggregation and sedimentation.

Example:

- A solvent has a surface tension of 42 $mJ \cdot m^{-2}$.
- The nanosheet surface energy is 40 $mJ \cdot m^{-2}$.

Result and meaning: Since $\gamma_s \approx \gamma_f$, the solvent is well matched for exfoliation, leading to stable dispersions. This indicates that exfoliation is likely to produce high yields of nanosheets without aggregation.

A2. Arrhenius growth kinetics in CVD

Formula:

$$r = k \cdot \exp(-E_a/RT)$$

Context: Growth rates in chemical vapor deposition (CVD) depend strongly on temperature. Engineers use Arrhenius behavior to optimize furnace conditions for throughput and quality.

Example:

$k = 1\times10^6\ nm\cdot s^{-1}$, $E_a = 1.2\times10^5\ J\cdot mol^{-1}$, $R = 8.314\ J\cdot mol^{-1}\cdot K^{-1}$, $T = 1273$ K (1000 °C)

Calculation:

$$r \approx 12.2\ nm\cdot s^{-1}$$

Result and meaning: At 1000 °C, deposition proceeds rapidly. If temperature is reduced by 100 °C, the rate would fall exponentially, showing the sensitivity of CVD growth to thermal control.

A3. Strain energy during transfer

Formula:

$$U = \tfrac{1}{2} \cdot E \cdot \varepsilon^2 \cdot V$$

Context: When transferring 2D films onto flexible substrates, strain energy accumulation may cause wrinkling or cracking.

Example:

$$E = 1\ \text{TPa},\ \varepsilon = 0.01,\ V = 1\times10^{-18}\ \text{m}^3$$

Calculation:

$$U = 5\times10^{-11}\ \text{J}$$

Result and meaning: Though tiny in absolute terms, this energy can overcome van der Waals adhesion between flakes and substrates. This explains why cracks appear even in nanoscopic films.

A4. Thermal conductivity in a nanosheet (Fourier's law)

Formula:

$$q = -k_{2D} A \frac{\Delta T}{L}$$

Context: Graphene is prized for its extreme thermal conductivity. Engineers use Fourier's law to estimate heat removal capacity in devices.

Example:

$$k_2D = 2000\ \text{W}\cdot\text{m}^{-1}\cdot\text{K}^{-1},\ A = 1\times10^{-12}\ \text{m}^2,\ \Delta T = 20\ \text{K},\ L = 1\times10^{-6}\ \text{m}$$

Calculation:

$$q = -0.04\ \text{W}$$

Result and meaning: A nanosheet can dissipate measurable heat, reinforcing why graphene is ideal for thermal interface materials in microelectronics.

A5. Composite modulus (Halpin–Tsai)

Formula:

$$E_c = E_m \frac{1 + \xi\eta\Phi}{1 - \eta\Phi}$$

Context: Predicting mechanical reinforcement guides filler loadings in polymer–graphene composites.

Example:

E_m = 3 GPa, E_f = 1000 GPa, φ = 0.01, ξ = 2

Calculation:

E_c ≈ 3.09 GPa

Result and meaning: Modulus increases by ~3% at only 1% filler loading, showing the efficiency of graphene reinforcement compared to conventional fillers.

A6. Percolation threshold conductivity

Formula:

$$\sigma = \sigma_0(\phi - \phi_c)^t$$

Context: Percolation theory explains when electrical networks form in composites containing conductive fillers.

Example:

σ_0 = 1000 $S\cdot m^{-1}$, φ = 0.01, φ_c = 0.005, t = 1.6

Calculation:

σ ≈ 0.32 $S\cdot m^{-1}$

Result and meaning: Conductivity appears only when filler exceeds φ_c. Here, conductivity is moderate but grows rapidly with increasing filler, guiding EMI shielding design.

A7. Joule heating in flexible heaters

Formula:

$$P = \frac{V^2}{R}$$

Context: Transparent heaters use thin conductive films to generate uniform heat. Power requirements determine safe voltage levels.

Example:

V = 5 V, R = 50 Ω

Calculation:

P = 0.5 W

Result and meaning: The heater consumes only half a watt, sufficient for mild heating. Scaling voltage or lowering Rs boosts power for de-icing or defogging.

A8. Responsivity of photodetector

Formula:

$$R = \frac{I_{ph}}{P_{opt}}$$

Context: Responsivity measures how effectively a photodetector converts light into current.

Example:

I_{ph} = 1 μA, P_{opt} = 10 nW

Calculation:

R = 100 $A{\cdot}W^{-1}$

Result and meaning: Responsivity of 100 $A{\cdot}W^{-1}$ shows strong amplification, outperforming conventional silicon photodiodes (~0.5 $A{\cdot}W^{-1}$). TMD devices thus enable ultrasensitive detection.

A9. Skin depth in EMI shielding

Formula:

$$\delta = \sqrt{\frac{2}{\omega\mu\sigma}}$$

With $\omega = 2\pi f$,

f is the frequency of the electromagnetic wave, measured in hertz (Hz).

Context: Skin depth governs how deeply electromagnetic waves penetrate conductors, critical for lightweight EMI shields.

Example:

$$f = 1\ \text{GHz},\ \sigma = 1\times10^{5}\ \text{S·m}^{-1},\ \mu \approx \mu_0 = 4\pi \times 10^{-7}\ \text{H·m}^{-1}$$

Calculation:

$$\delta \approx 50\ \mu\text{m}$$

Result and meaning: At GHz frequencies, only the top tens of microns contribute to shielding. Hence thin MXene films suffice for strong EMI attenuation.

A10. Butler–Volmer electrode kinetics

Formula:

$$i = i_0\,[e^{anF\eta/RT} - e^{-(1-a)nF\eta/RT}]$$

Context: This equation governs electrocatalytic reactions, essential for energy devices like hydrogen evolution electrodes.

Example:

$$i_0 = 1\times10^{-3}\ \text{A·m}^{-2},\ \alpha = 0.5,\ n = 2,\ \eta = 0.1\ \text{V}$$

Calculation:

$$i \approx 0.049\ \text{A·m}^{-2}$$

Result and meaning: Even modest overpotentials generate significant current, showing how catalytic activity is highly sensitive to electrode material and surface engineering.

A11. Permeance in membranes

Formula:

$$P = \frac{J}{\Delta p}$$

Context: Permeance benchmarks water or gas transport through membranes, balancing flux with selectivity.

Example:

$J = 1\times10^{-5}$ mol·m^{-2}·s^{-1}, $\Delta p = 1\times10^{5}$ Pa

Calculation:

$P = 1\times10^{-10}$ mol·m^{-2}·s^{-1}·Pa^{-1}

Result and meaning: This value matches GO membranes, offering high flux while rejecting salts. Engineers use such results to compare candidate membranes.

A12. Electromigration lifetime (Black's law)

Formula:

$$t_f = AJ^{-n}e^{E_a/k_B T}$$

Context: Electromigration limits current-carrying capacity in nanoscale conductors.

Example:

$J = 1\times10^{10}$ A·m^{-2}, $n = 2$, $E_a = 0.8$ eV, $T = 373$ K

Calculation:

$t_f \approx 1.6\times10^{-14}$ s

Result and meaning: Lifetime collapses at extreme current densities, illustrating the importance of safe operating margins in 2D electronic devices.

A13. Impact factor in lifecycle assessment

Formula:

$$IF = \sum_i E_i CF_i$$

Context: Lifecycle assessment quantifies environmental impacts by aggregating emissions with their impact factors.

Example:

CO_2 = 1 kg, CF = 1; SO_2 = 0.01 kg, CF = 120

Calculation:

IF = 2.2 kg CO_2 eq

Result and meaning: Even small emissions of SO_2 dominate the impact. Engineers must track multiple pollutants, not just CO_2, to evaluate sustainability.

Conclusion

These worked examples contextualize equations by showing why they matter in design, how to calculate with real values, and what the numbers mean in practice. From exfoliation solvents to EMI shielding and lifecycle impact, the results illustrate the practical decision-making frameworks that engineers apply in 2D material development.

Bibliography

1. Anasori, B., Lukatskaya, M.R. and Gogotsi, Y. (2017) 2D metal carbides and nitrides (MXenes) for energy storage. *Nature Reviews Materials*, 2(2), p.16098.
2. Bae, S., Kim, H., Lee, Y. *et al.* (2010) Roll-to-roll production of 30-inch graphene films for transparent electrodes. *Nature Nanotechnology*, 5(8), pp. 574–578.
3. Balandin, A.A. (2011) Thermal properties of graphene and nanostructured carbon materials. *Nature Materials*, 10(8), pp. 569–581.
4. Berman, D., Erdemir, A. and Sumant, A.V. (2015) Graphene: a new emerging lubricant. *Materials Today*, 17(1), pp. 31–42.
5. Bonaccorso, F., Sun, Z., Hasan, T. and Ferrari, A.C. (2010) Graphene photonics and optoelectronics. *Nature Photonics*, 4(9), pp. 611–622.
6. Cahill, D.G. (2004) Analysis of heat flow in layered structures for time-domain thermoreflectance. *Review of Scientific Instruments*, 75(12), pp. 5119–5122.
7. Chen, S., Brown, L., Levendorf, M. *et al.* (2012) Oxidation resistance of graphene-coated Cu and Al. *ACS Nano*, 5(2), pp. 1321–1327.
8. Coleman, J.N., Lotya, M., O'Neill, A. *et al.* (2011) Two-dimensional nanosheets produced by liquid exfoliation of layered materials. *Science*, 331(6017), pp. 568–571.
9. Dreyer, D.R., Park, S., Bielawski, C.W. and Ruoff, R.S. (2010) The chemistry of graphene oxide. *Chemical Society Reviews*, 39(1), pp. 228–240.
10. Ferrari, A.C. and Basko, D.M. (2013) Raman spectroscopy as a versatile tool for studying the properties of graphene. *Nature Nanotechnology*, 8(4), pp. 235–246.
11. Geim, A.K. and Grigorieva, I.V. (2013) Van der Waals heterostructures. *Nature*, 499(7459), pp. 419–425.
12. Geim, A.K. and Novoselov, K.S. (2007) The rise of graphene. *Nature Materials*, 6(3), pp. 183–191.
13. Gogotsi, Y. and Anasori, B. (2019) The rise of MXenes. *ACS Nano*, 13(8), pp. 8491–8494.
14. Graphene Flagship (2020) *Graphene in commercial products*. Available at: https://graphene-flagship.eu
15. Haacke, G. (1976) New figure of merit for transparent conductors. *Journal of Applied Physics*, 47(9), pp. 4086–4089.
16. Hunter, R.J. (1981) *Zeta potential in colloid science: Principles and applications*. London: Academic Press.
17. IDTechEx (2022) *Graphene, 2D materials and carbon nanotubes: Market forecasts 2022–2032*. Cambridge: IDTechEx.

18. IEC (2022) *IEC TS 62607-6-7: Nanomanufacturing – Key control characteristics – Graphene-based material – Sheet resistance: van der Pauw method*. Geneva: International Electrotechnical Commission.
19. IEC (2023) *IEC TS 62607-6-18: Nanomanufacturing – Key control characteristics – Graphene-based material – Functional groups: TGA–FTIR*. Geneva: International Electrotechnical Commission.
20. ISO (2024) *ISO/TS 80004-13: Nanotechnologies – Vocabulary – Part 13: Graphene and other two-dimensional materials*. Geneva: International Organization for Standardization.
21. Jaramillo, T.F., Jørgensen, K.P., Bonde, J., Nielsen, J.H., Horch, S. and Chorkendorff, I. (2007) Identification of active edge sites for electrochemical H_2 evolution on MoS_2 nanocatalysts. *Science*, 317(5834), pp. 100–102.
22. Kang, J., Kim, H., Kim, K.S. *et al.* (2011) High-performance graphene-based transparent flexible heaters. *Nano Letters*, 11(12), pp. 5154–5161.
23. Kim, K.S., Zhao, Y., Jang, H. *et al.* (2011) Large-scale pattern growth of graphene films for stretchable transparent electrodes. *Nature*, 457(7230), pp. 706–710.
24. Li, L., Yu, Y., Ye, G.J. *et al.* (2014) Black phosphorus field-effect transistors. *Nature Nanotechnology*, 9(5), pp. 372–377.
25. Li, X., Cai, W., An, J. *et al.* (2009) Large-area synthesis of high-quality and uniform graphene films on copper foils. *Science*, 324(5932), pp. 1312–1314.
26. Ling, Z., Ren, C.E., Zhao, M.Q. *et al.* (2014) Flexible and conductive MXene films and nanocomposites with high capacitance. *Proceedings of the National Academy of Sciences*, 111(47), pp. 16676–16681.
27. Lopez-Sanchez, O., Lembke, D., Kayci, M., Radenovic, A. and Kis, A. (2013) Ultrasensitive photodetectors based on monolayer MoS_2. *Nature Nanotechnology*, 8(7), pp. 497–501.
28. Lukatskaya, M.R., Mashtalir, O., Ren, C.E. *et al.* (2013) Cation intercalation and high volumetric capacitance of two-dimensional titanium carbid. *Science*, 341(6153), pp. 1502–1505.
29. Mak, K.F., Lee, C., Hone, J., Shan, J. and Heinz, T.F. (2010) Atomically thin MoS_2: A new direct-gap semiconductor. *Physical Review Letters*, 105(13), 136805.
30. Nair, R.R., Blake, P., Grigorenko, A.N. *et al.* (2008) Fine structure constant defines visual transparency of graphene. *Science*, 320(5881), p. 1308.
31. Nair, R.R., Wu, H.A., Jayaram, P.N., Grigorieva, I.V. and Geim, A.K. (2012) Unimpeded permeation of water through helium-leak-tight graphene-based membranes. *Science*, 335(6067), pp. 442–444.
32. Naguib, M., Kurtoglu, M., Presser, V. *et al.* (2011) Two-dimensional nanocrystals produced by exfoliation of Ti_3AlC_2. *Advanced Materials*, 23(37), pp. 4248–4253.
33. Novoselov, K.S., Geim, A.K., Morozov, S.V. *et al.* (2004) Electric field effect in atomically thin carbon films. *Science*, 306(5696), pp. 666–669.

34. Novoselov, K.S., Geim, A.K., Morozov, S.V. *et al.* (2005) Two-dimensional gas of massless Dirac fermions in graphene. *Nature*, 438(7065), pp. 197–200.
35. Potts, J.R., Dreyer, D.R., Bielawski, C.W. and Ruoff, R.S. (2011) Graphene-based polymer nanocomposites. *Polymer*, 52(1), pp. 5–25.
36. Radisavljevic, B., Radenovic, A., Brivio, J., Giacometti, V. and Kis, A. (2011) Single-layer MoS_2 transistors. *Nature Nanotechnology*, 6(3), pp. 147–150.
37. Reina, A., Jia, X., Ho, J. *et al.* (2009) Large area, few-layer graphene films on arbitrary substrates by chemical vapor deposition. *Nano Letters*, 9(1), pp. 30–35.
38. Sarycheva, A., Makaryan, T., Maleski, K. *et al.* (2018) Two-dimensional titanium carbide (MXene) as surface-enhanced Raman scattering substrate. *ACS Applied Materials & Interfaces*, 10(11), pp. 9161–9169.
39. Schedin, F., Geim, A.K., Morozov, S.V. *et al.* (2007) 'Detection of individual gas molecules adsorbed on graphene', *Nature Materials*, 6(9), pp. 652–655.
40. Schinwald, A., Murphy, F.A., Jones, A., MacNee, W. and Donaldson, K. (2012) Graphene-based nanoplatelets: a new risk to the respiratory system as a consequence of their unusual aerodynamic characteristics. *ACS Nano*, 6(1), pp. 736–746.
41. Seabra, A.B., Paula, A.J., de Lima, R., Alves, O.L. and Durán, N. (2014) Nanotoxicity of graphene and graphene oxide. *Chemical Research in Toxicology*, 27(2), pp. 159–168.
42. Stankovich, S., Dikin, D.A., Dommett, G.H.B. *et al.* (2006) Graphene-based composite materials. *Nature*, 442(7100), pp. 282–286.
43. Sun, J., Zheng, J., Zhang, X. *et al.* (2017) Two-dimensional phosphorene-based materials for separation applications. *Nature Communications*, 8, p. 14969.
44. Tamagnone, M., Gomez-Diaz, J.S., Mosig, J.R. and Perruisseau-Carrier, J. (2012) Analysis and design of terahertz antennas based on plasmonic resonant graphene sheets. *Applied Physics Letters*, 101(21), 214102.
45. Watanabe, K., Taniguchi, T. and Kanda, H. (2004) Direct-bandgap properties and evidence for ultraviolet lasing of hexagonal boron nitride single crystal. *Nature Materials*, 3(6), pp. 404–409.
46. Xiao, D., Liu, G.B., Feng, W., Xu, X. and Yao, W. (2012) Coupled spin and valley physics in monolayers of MoS_2 and other group-VI dichalcogenides. *Physical Review Letters*, 108(19), 196802.
47. Xie, Y., Naguib, M., Mochalin, V.N. *et al.* (2014) Role of surface structure on Li-ion energy storage capacity of two-dimensional transition-metal carbides. *Nature Materials*, 13(6), pp. 541–549.
48. Yu, A., Ramesh, P., Sun, X. *et al.* (2008) Enhanced thermal conductivity in a hybrid graphite nanoplatelet – carbon nanotube filler for epoxy composites. *Advanced Materials*, 20(24), pp. 4740–4744.

49. Young, R.J., Kinloch, I.A., Gong, L. and Novoselov, K.S. (2012) The mechanics of graphene nanocomposites: A review. *Composites Science and Technology*, 72(12), pp. 1459–1476.
50. Zhao, J., Liu, H., Zhu, L., Liu, Z. and Wang, X. (2011) Electrochemical exfoliation of graphene: New facets and potential applications. *Nano Research*, 4(10), pp. 1010–1018.
51. Zhao, J., Zhang, H., Liu, G. *et al.* (2019) MXene nanosheets as high-performance solid lubricants. *Advanced Materials*, 31(4), p.1805435.
52. Zhou, B., Zhang, C., Sun, T. *et al.* (2019) Highly conductive and flexible Ti_3C_2Tx MXene films for electromagnetic interference shielding. *ACS Nano*, 13(4), pp. 4523–4530.
53. Figure 1: 3113Ian at English Wikipedia, CC BY-SA 3.0 <https://creativecommons.org/licenses/by-sa/3.0>, via Wikimedia Commons
54. Figure 2: Nesbit1973, CC BY-SA 4.0 <https://creativecommons.org/licenses/by-sa/4.0>, via Wikimedia Commons
55. Figure 3: ECTran71, CC BY-SA 4.0 <https://creativecommons.org/licenses/by-sa/4.0>, via Wikimedia Commons

Educational Use Only

The content of this course is provided for educational purposes only. While every effort has been made to ensure the accuracy and reliability of the information presented, the author or publisher makes no guarantees regarding the completeness or applicability of the information to specific professional practices. Users are advised to consult additional resources and exercise professional judgment when applying the knowledge contained in this course.

Use of AI Generated Content

The continuing education (CE) courses offered on this platform are developed using advanced artificial intelligence (AI) methodologies to generate high-quality, text-based instructional content.

These courses are primarily designed to provide in-depth knowledge on engineering and technical subjects with minimal or no imagery, focusing on comprehensive textual explanations to convey concepts effectively.

While every effort is made to ensure accuracy, clarity, and compliance with professional standards, the nature of AI-assisted content generation means that occasional errors or inconsistencies may occur. Users are encouraged to critically evaluate the material and verify key technical details as needed. Additionally, these courses do not include interactive elements or extensive visual aids such as diagrams, charts, or illustrations unless explicitly stated.

By enrolling in and using these courses, participants acknowledge and accept that the content is primarily text-based and generated through AI-assisted processes. The course provider assumes no liability for any inaccuracies or omissions and advises professionals to apply their own judgment and expertise when utilizing course materials in practical applications.